Journal of Applied Engineering and Technological Science
Vol 7(1) 2025: 101-118

FABRICATION AND MEASUREMENT OF A CIRCULARLY POLARIZED ALL-METAL PATCH ARRAY AND SINGLE PRS LAYER-BASED FABRY-PEROT ANTENNA FOR NASA INTERPLANETARY CUBESAT MISSIONS

Fouad Omari[1], Boutaina Benhmimou[2], Nancy Gupta[3], Khalid El Khadiri[4], Rachid Ahl Laamara[5], Mohamed El Bakkali[6*]

LPHE-MS, Faculty of Sciences, University Mohammed V in Rabat (UM5), Rabat, Morocco[1256]

ECE Department, Lyallpur Khalsa College Technical Campus, Jalandhar, Punjab, India[3]

Department of Physics, Faculty of Sciences El Jadida, University Chouaib Doukkali, El Jadida, Morocco[46]

mohamed.elbakkali1617@gmail.com

Received: 30 December 2024, Revised: 21 May 2025, Accepted: 25 August 2025
**Corresponding Author*

ABSTRACT
When it comes to pushing the limits of small-scale technologies for interplanetary space missions, NASA has demonstrated that the dream is achievable. NASA has launched a number of interplanetary CubeSat missions, including as MarCO A and B, INSPIRE, LOGIC, and LunaH-map CubeSats, successfully during the past 10 years. Since the antennas of these NASA-certified satellites are responsible for defining the range of communication with Earth, they are the main topic of this study. A high gain and circularly polarized all-metal patch array with PRS-based Fabry Perot antenna is proposed in this paper for NASA's interplanetary CubeSat missions. The strength of this approach stems from its dependence on a wholly novel concept for developing a durable antenna that is harmoniously compatible with NASA's goals. The resulting all-metal patch array was well-fabricated and tested in an anechoic chamber and using a VNA, and showed measured realized gain of 35.84 dBi and AR of 1.629 dB at 11.5 GHz with 3dB-AR bandwidth higher than 3 GHz. Additionally, the Fabry-Perot design enhances the gains, achieves AR of 0.29 dB at 12.1 GHz, and exhibits RHCP and LHCP making this new technique as suitable candidates for NASA's interplanetary CubeSat missions.
Keywords: *Fabry Perot Antennas, High Gain Antennas, LHCP and RHCP, NASA Interplanetary CubeSats.*

1. Introduction

The solar system contains tens of thousands of microscopic objects as small as ten kilometers, with many more in the main asteroid belt. We do not know much about these tiny creatures; the ephemerides are not accurate enough for mission guidance, and the bodies are so small and dark that a spacecraft journeying to them may pass by undetected. Furthermore, only space organizations and their engineers and scientists with budgets in the hundreds of millions of dollars can carry out solar system exploration missions (Tollefson et al., 2021; Kramer, 2021). Although their achievements are extensive, extremely complex, and truly extraordinary, the exorbitant expense slows down the rate of significant discoveries (Autry, 2024). To deal with that, having several tiny spacecraft that concentrate on basic tasks rather than one giant spacecraft with extremely sophisticated multitasking capabilities is an alternate possibility. Using CubeSats as stepping stones to create the emerging idea of a scientific interplanetary CubeSat for proximity operations, cruise, or other activities near a small body of the solar system (such as an irregular satellite, comet, or asteroid) is a plausible alternative (Freeman, 2020). Its purpose is to use imaging and radio science techniques to describe the interior structure, shape, and gravitational field of the body. Interplanetary CubeSats provide a possibility to carry out targeted scientific studies throughout the inner Solar System at a tenfold lower cost than standard missions. They provide a compelling road ahead for the development of brief, concentrated science missions that serve as prototypes for bigger, longer missions. They will pave the way for a comparable transformation in access to space and new discoveries beyond Earth. With a large number of new

missions planned, they are becoming increasingly popular (Tanaka et al., 2024) (Lambright, 2024).

Interplanetary CubeSats are particularly built to travel deep space using the CubeSat standards and the availability of commercial components created for low Earth orbit (LEO) missions. They vary because their orbits carry them far from our mother planet, Earth, and its familiar surroundings. In LEO, a CubeSat must be very complicated in order to power and sustain electronics and other equipment, maintain specific orientations, and respond to orders, all while obtaining and reporting health status and data to achieve mission objectives. All of these features must be available after a CubeSat's orbit departs from Earth's vicinity, although achieving some of these features calls for new methods and complexity. The majority of CubeSats in Earth orbit, particularly LEO, reach their intended orbit in a matter of minutes after they begin operations. For most interplanetary CubeSats, the majority of the mission and its complexity will be tested when transitioning from the mission's launch orbit to one or more destination orbits where the CubeSat may carry out its planned goal by obtaining data unavailable from elsewhere. In this context, NASA created a number of interplanetary CubeSats, such as CAPSTONE, Lunar IceCube, Lunar Flashlight, and LunaH-Map, using the sensible principle that they should have sufficient bandwidth to enable software upgrades for spacecraft flight within an acceptable timescale (Thompson et al., 2022); refer to Fig. 1. For example, the NASA's lunar mission concept aims to place a fleet of CubeSats in orbit around the Moon to address scientific questions about space weathering, the origins of planetary magnetism, distributions, and migration processes of surface water on airless bodies, and the physics of small-scale magnetospheres. It employs a revolutionary "mother-with-many-children" design to launch its CubeSats into a low, circular, polar orbit around the moon. The mother ship sends several CubeSats on impact paths into the cores of lunar magnetic anomalies to monitor magnetic fields and proton flows in real time, down to the last tens of milliseconds. They would subsequently deploy a second set of CubeSats to monitor neutron fluxes in a polar orbit with a periapsis above the South Pole.

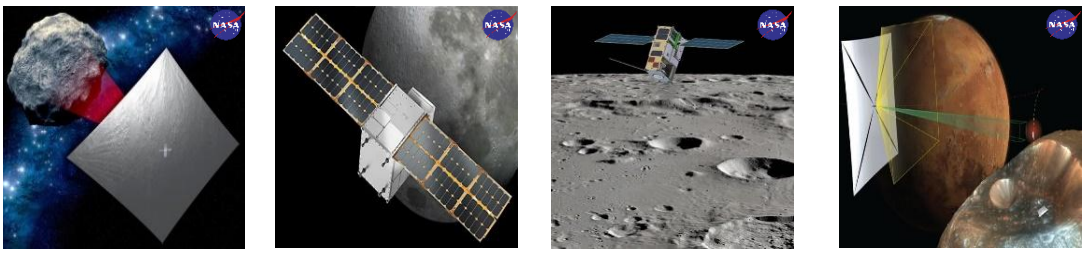

a). NASA's NEA Scout CubeSat with its solar sail deployed as it characterizes a near-Earth asteroid.

b). NASA's CAPSTONE mission: The first CubeSat flew in cis lunar space to offer an innovative option for Artemis' Gateway.

c). NASA's Lunar IceCube mission to prospect for waterice and other lunar volatiles from lunar

NASA's Interplanetary CubeSats retrieving a sample from one of the Mars two moons, Phobos or Deimos.

Fig. 1. Most potent NASA' interplanetary CubeSat initiatives.

Because of this, interplanetary CubeSats differ significantly from LEO missions in three key technology areas: telecommunications, radiation tolerance, and propulsion. These differences are essential, yet they necessitate modifications to nearly all satellite subsystems. Due to the existence of propulsion and the necessity for demanding telecommunications systems, interplanetary CubeSats have higher power needs than LEO CubeSats. As a result, they require power systems with lower power modes and larger energy storage capacities (Campana, 2023). In addition to that, more sophisticated thermal control technologies are frequently required to disperse surplus heat into deep space due to increased power level requirements. Interplanetary CubeSats also need radiation tolerance techniques due to their location outside of Earth's magnetosphere. To prevent wheel saturation problems outside of Earth's geomagnetic field, interplanetary CubeSats' attitude determination and control systems (ADCS) require a combination of conventional control systems and propulsion. Moreover, agile algorithms are required to enable autonomous onboard operations since interplanetary missions have less frequent ground interaction than low Earth orbit missions. Usually compared to LEO missions, interplanetary CubeSats need different and more complicated system designs and need to use

different and more advanced ground station technologies (Omari et al., 2023). Another significant distinction between interplanetary and low-Earth orbit missions is the telecommunications systems. Compared to LEO CubeSats, interplanetary CubeSats must navigate through more complex environments and across greater distances. Because of this, designing telecommunications systems for interplanetary missions is quite difficult, and major progress is now underway in the fields of radio, antenna, and earth segment architecture design (Boutaina et al., 2024).

This means that high gain antennas on the spaceship and the utilization of wide apertures with sensitive electronics on the earth segments are necessary to close a telecommunication link over interplanetary distances. Data rates attained by interplanetary CubeSats on long space missions are proportional to distance, since they often employ the most effective technology (NASA Deep Space Network and high gain antennas). When it comes to the design of telecommunication systems, the only degrees of freedom are wavelength and antenna size because deep space transceivers have restricted output power (usually 4–7 W). The trade-off is that aiming toward Earth might become difficult due to the smaller transmit antenna beamwidths (associated with higher frequencies). Note that the ADCS systems are presently available for CubeSats and can provide the platform stability and pointing precision required to operate these high-frequency telecommunications systems. To address these issues, this project proposes a novel interplanetary spacecraft antenna approach based on the use of all-metal patch array and Fabry-Perot configurations (Omari et al., 2023) (El Bakkali et al., 2021). Both antenna systems are well-configured, optimized, and shrunk to be geometrically, mechanically, and electrically suitable for NASA's interplanetary CubeSats. This project has been designed with the highly harsh circumstances that may exist in the environment of NASA's interplanetary missions. This project is being developed on the campuses of two Moroccan universities, University Mohammed V in Rabat (UM5) and Chouaib Doukkali in El Jadida, in order to support and participate in NASA's recent advancement of deep space technologies, as well as to open doors for the rest of the world's engineers to join NASA in supporting and participating in understanding how the universe works.

The following parts provide the highlights of this work. Section 2 presents a detailed geometric analysis of the established strategy. Section 3 thoroughly discusses and analyzes all obtained performances. Section 4 describes the antenna fabrication and the results of experimental measurements using a VNA and an anechoic chamber. The overall findings are well compared, particularly with more than 20 comparable Fabry-Perot antenna designs developed by the scientific community in terms of appropriateness for NASA's interplanetary CubeSats. Section 6 completes the planned study.

2. Antenna Design and Geometrical Description

The first option for increased stiffness and improved performance at Ku-band CubeSat frequencies was a lightweight all-metal patch array with seven horizontally stacked patches. The HFSS software's FEM and Quasi Newton's technique were used to design, optimize, and miniaturize this antenna, resulting in a final volume of no more than $4.51\times0.8\times0.08\lambda_0^3$, see Fig.1(e).We then worked on adopting two models of the same prior antenna system with a 90-degree angle between them in order to achieve circular polarization while lowering the antenna size in a manner acceptable with the missions of long-range cube satellites. A third and fourth models of the same antenna were added perpendicularly, each time at a 90-degree angle, in order to improve the antenna capacity while maintaining the same objectives (see fig. 1(c)). The resultant configuration, which is made up of four identical models of the prior antenna arranged perpendicular to one another, is compact and flat, has a small area and a small volume, and provides circular polarization simultaneously. Besides that, and in order to create a robust, rigid, and circularly polarized metal antenna that is compact in size and geometrically compatible with the smallest interplanetary cube satellites, a model of the same previous antenna was added to the four sides of the finished antenna system (Fig.1(c)) in a flat, parallel, and compact shape while taking into account the coordinates of an interplanetary cube satellite mission, see Fig. 1(d) and (f). A 50Ω coaxial probe is welded in the midst of an all-metal patch array to maximize gain and preserve good return loss and low axial ratio at 12.1 GHz. Its copper construction, physical

volume of $4.5\lambda_0 \times 6.13\lambda_0 \times 0.08\lambda_0$, and RHCP and LHCP polarizations make it ideal for interplanetary CubeSat missions at Ku-band.

To improve the impedance bandwidth, axial ratio, and impedance matching of the optimized all-metal patch array that is dual band, an array of 34×58 partially selective surface (PRS)unit cells is used to create a circularly polarized Fabry Perot antenna with a wide impedance bandwidth and good impedance matching at 12.1 GHz, see fig. 2. The FP antenna design is also improved using the quasi-Newtonian method, which is contained in HFSS packages (Patidar et al., 2024).

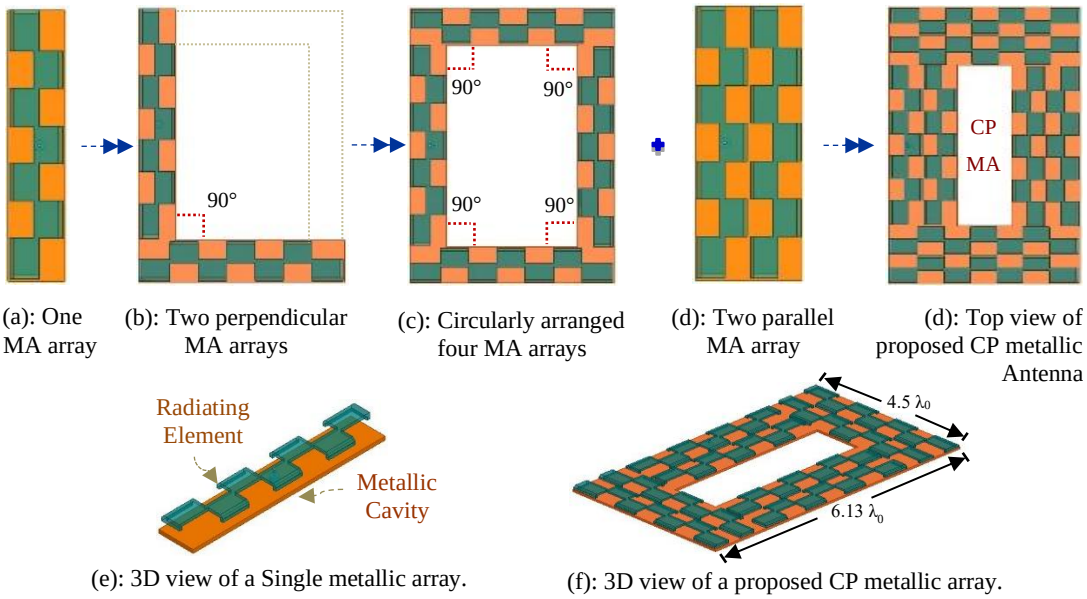

(a): One MA array (b): Two perpendicular MA arrays (c): Circularly arranged four MA arrays (d): Two parallel MA array (d): Top view of proposed CP metallic Antenna

(e): 3D view of a Single metallic array. (f): 3D view of a proposed CP metallic array.

Fig. 1. Configuration and evolution of developed CP all-metal antenna array.

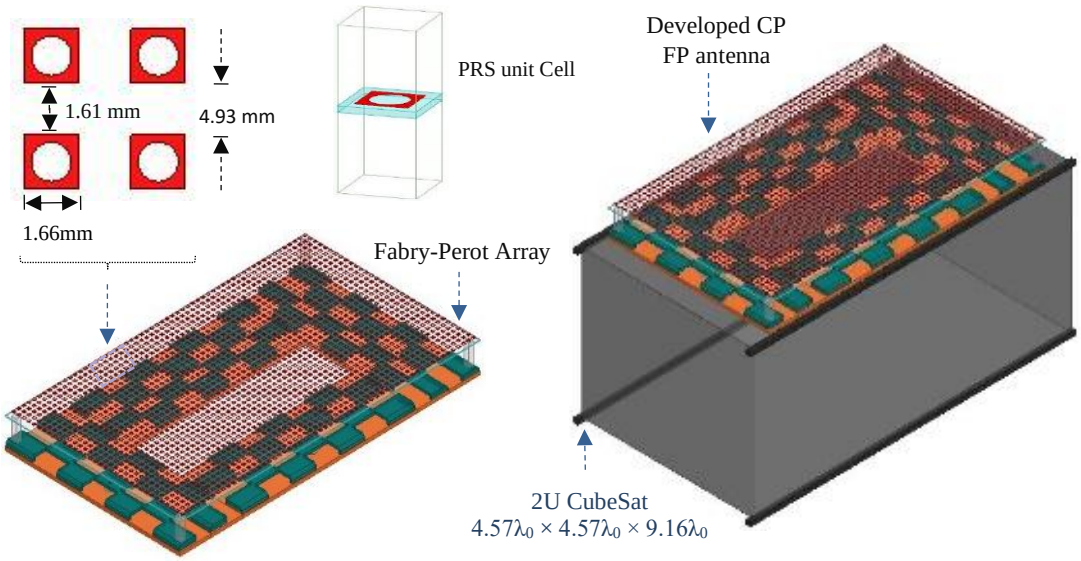

(a) 3D HFSS layout of developed CP Fabry-Perot antenna (b) 3D Model of 2U CubeSat spacecraft: 2U CubeSat + developed CP Fabry-Perot antenna

Fig. 2. Geometry of developed Fabry Perot antenna and 2U CubeSat configuration.

The Fabry-Perot antenna has the same total size of $4.5\lambda_0 \times 6.13\lambda_0$ and is placed at distance of 1.04 λ_0 above the source antenna. It is constructed using an array of PRS unit cells, which are mounted above Rogers 5880 substrate. The PRS unit cell has square shape and length of 2 mm. all radiating elements of proposed CP Fabry Perot antenna are made of copper and are welded with the CubeSat chassis. In terms of geometry, weight, size, cost, stiffness and power consumption, the proposed Fabry Perot antenna is mechanically and geometrically very suitable for interplanetary communications using 2U, 3U and 6U CubeSats.

3. Analysis of Calculated Results

As previously indicated, the design and optimization of a single metallic array that is appropriate for all CubeSat designs, even the tiniest ones, was the first step in this technique. According to Fig. 3, it operates over an ultra-wide impedance bandwidth of 75.3% (10.43–12.69 GHz) and provides a reflection coefficient that is considerably below -20 dB at 12.1 GHz, with the lowest being -29.15 dB at 10.77 GHz. Its VSWR coefficient supports these requirements, with a bandwidth of 77% (10.41-12.72 GHz), a low of almost one at 10.77 GHz, and a modest value of 1.28 at 12.1 GHz. Furthermore, Fig. 4 demonstrates that this design exhibits uniform surface current and E-field distributions, which support and explain its very directional radiation pattern at 12.1 GHz.

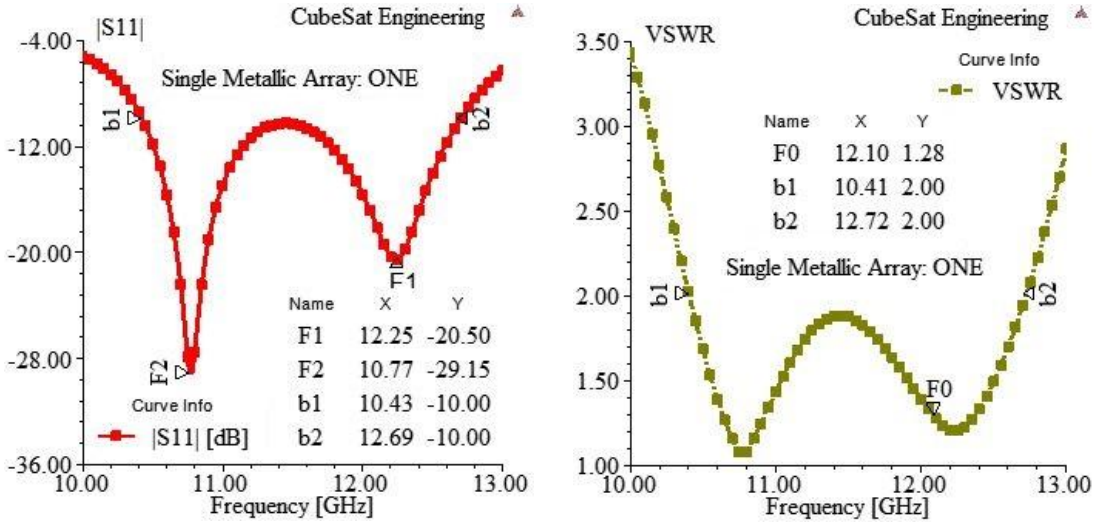

a). |S11| coefficient vs. frequency. b). VSWR coefficient vs. frequency.

Fig. 3. |S11| and VSWR coefficients of proposed single metallic array vs. frequency.

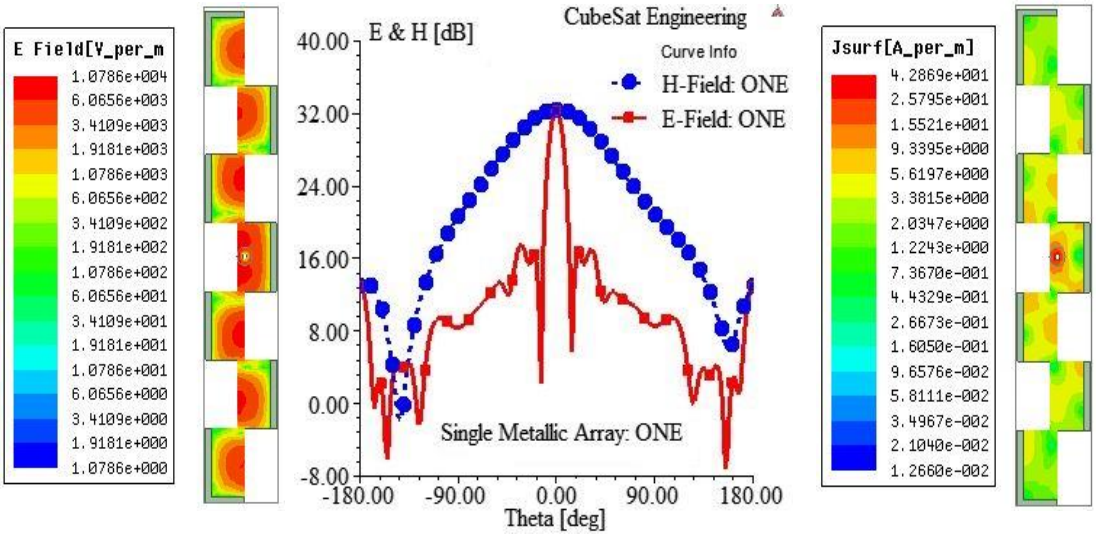

a) Distribution of E-field. b) E- and H-Fields.d). c) Distribution of surface current.

Fig. 4. E-field and Surface Current distributions and 2D radiation pattern of proposed single metallic array at 12.1 GHz.

As seen in Fig. 5, the greatest amounts of E-field and, consequently, electric power are radiated into space outside the spacecraft box in a similar manner, resulting in a peak gain of 14.59 dBi at 12.07 GHz and a 3dB gain bandwidth greater than 1.0 GHz. It exhibits linear polarization, a good beamwidth angle of around 12.1 GHz, and a unidirectional radiation pattern. This indicates that it is an excellent option for advanced LEO CubeSat missions, particularly when employing the smallest spacecraft, because to its metallic design, lightweight, high rigidity, and

compact size, which allows it to give up a lot of area on the CubeSat body for other satellite equipment. Because nuclear batteries can run safely for thousands of years, the current advancements in electric power engineering at American institutions, such as NASA's Jet Propulsion Laboratory (JPL), have overcome the limitation of spacecraft size if its antenna systems perform well, such as this single metallic patch array. However, deep space missions such as NASA's interplanetary CubeSat programs prefer higher performances in terms of realized gains and circular polarization to ensure radio links with the mother spacecraft and NASA earth segments. To fulfill the goal of interplanetary missions, the created techniques are evolved into steps 2 and 3 to attain the best performance achievable. Fig. 6 demonstrates that the second-step all-metal patch array is dual-band, functioning in two effective bands of 10.4-11.3 GHz (30%) and 11.6-12.8 GHz (40%). It has a VSWR of 1.2 at 12.1 GHz and a reflection coefficient of less than -25 dB around the same frequency.

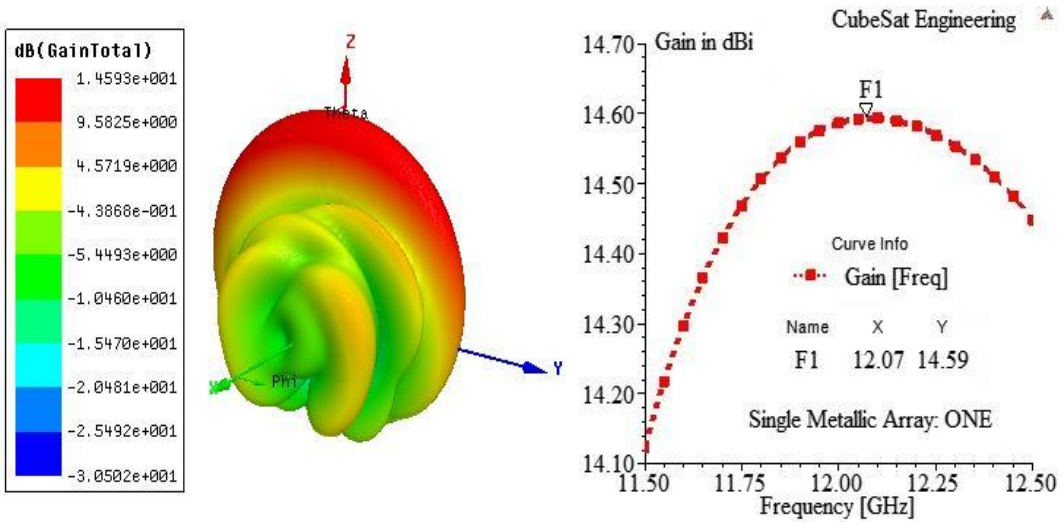

a) 3D gain at 12.10 GHz. a) Gain vs Frequency.

Fig. 5. Peak Gain of proposed Single metallic antenna array.

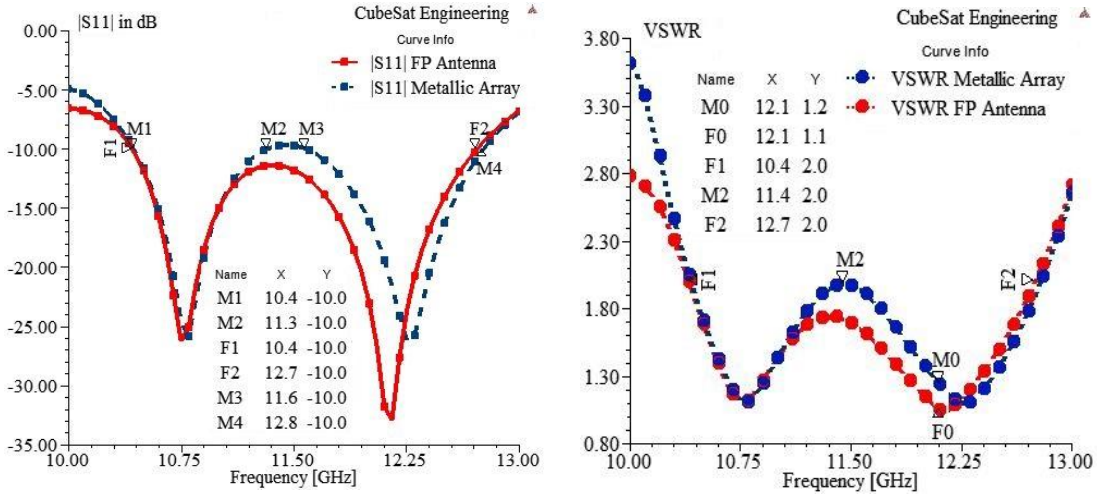

a) |S11| vs frequency b) VSWR vs frequency

Fig. 6. |S11| of the CP FP antenna and the fully metallic array vs. frequency.

These performances are all improved by achieving impedance matching around 12.1 GHz using the single PRS-based Fabry-Perot antenna built in the third stage of this investigation (see Figs. 6 and 7). The Fabry-Perot antenna system merges the two effective bands of the all-metal patch array into a single ultra-wide impedance bandwidth spanning 10.4 to 12.7 GHz (76.6%), with the lowest reflection coefficients and minimum VSWR parameter at practically all frequencies. It produces a |S11| of around -35 dB and a VSWR of 1.1 at 12.1 GHz. Furthermore, it has an input impedance of 49.9-j0.1 at 12.1 instead of the all-metal patch array's 55.3+j8.3 at the

same frequency. Hence, it improves the input impedance of developed fully metallic antenna array to present good impedance matching at 12.10 GHz and then minimize the excitation losses.

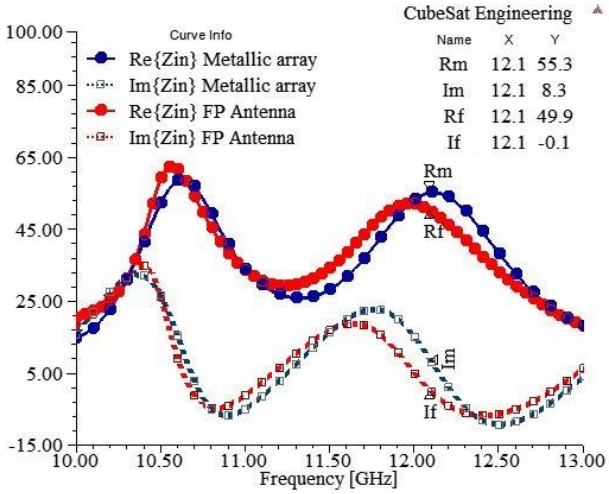

Fig. 7. Input impedance of CP FP antenna and the all-metal patch array vs. frequency.

Furthermore, both the all-metal patch array and the Fabry-Perot antenna radiate unidirectionally, providing RHCP and LHCP capabilities at 12.1 GHz. The LHCP and RHCP achieved gains at 12.1 GHz are 20.73 dBi and 17.19 dBi for the all-metal patch array alone, and 21.27 dBi and 18.04 dBi for the Fabry-Perot antenna system, respectively (see Figs. 8 and 9). This indicates that, in addition to the bandwidth and impedance matching improvements made by the optimized PRS-based Fabry-Perot system, this one enhances the realized gains of LHCP and RHCP in the same direction and at the same point of frequency. These suggestions are supported by the findings of realized gain and axial ratio, which are shown as a function of frequency in Fig. 10.

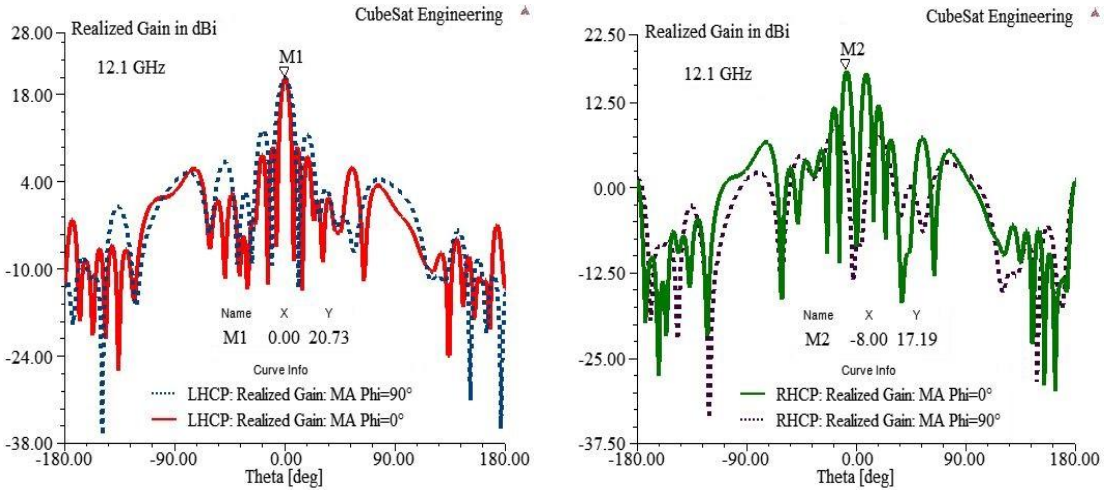

a) LHCP realized gain. b) RHCP realized gain.

Fig. 8. LHCP and RHCP realized gains of the fully metallic array at 12.1 GHz.

Furthermore, both the metal-patch array and the Fabry-Perot designs have attained gains well higher than 20.5 dBi and an axial ratio well below 0.6 dB throughout a wide frequency range (>300 MHz).This results in large 3dBi gain bandwidths for both designs with negligible polarization and excitation losses, allowing for some extra benefits in the event of interaction with any unexpected surprises from the harsh environment of interplanetary missions. It also leads to the maintenance of a continuous bidirectional communication between the CubeSat and the mother spacecraft, as well as NASA's segments on Earth, allowing for the advancement of space

exploration science and, ultimately, our comprehension of the universe. This demonstrates how the antenna performances of the mother spacecraft and its children is too critical for NASA's interplanetary missions, which are generally human-made projects.

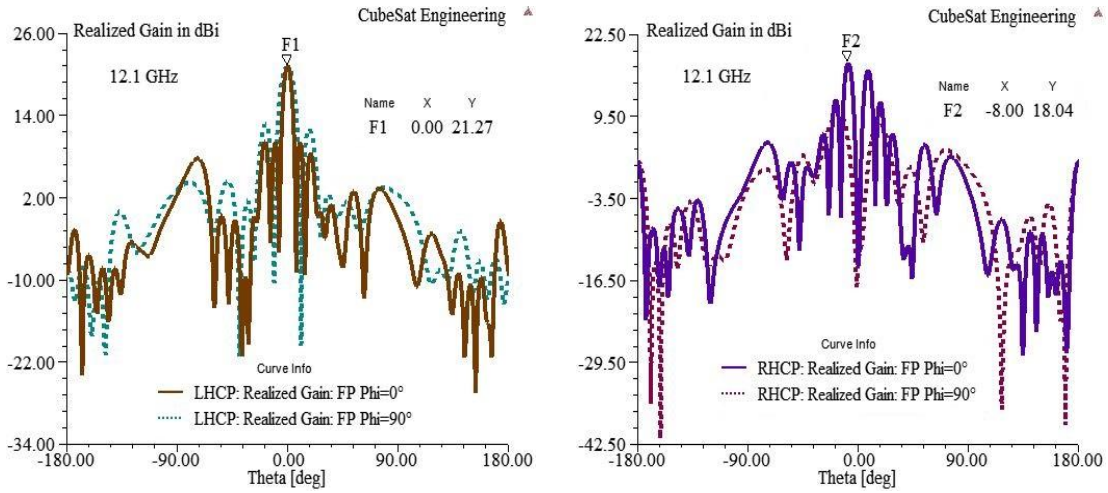

a) LHCP realized gain. b) RHCP realized gain.

Fig. 9. LHCP and RHCP realized gains of the Fabry-Perot antenna at 12.10 GHz.

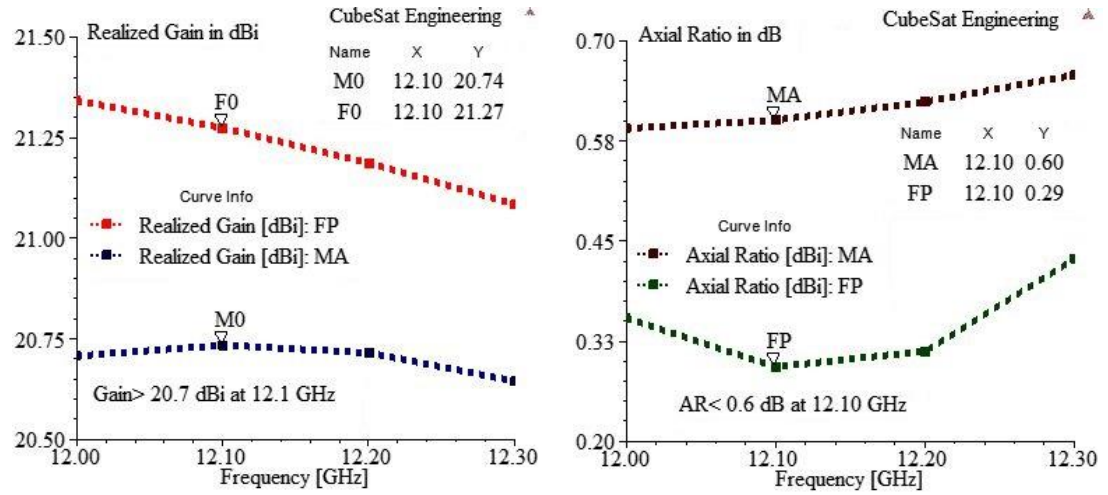

a) Realized gain vs. frequency. b) Axial ratio vs. frequency.

Fig. 10. Realized gain and axial ratio of developed Fabry-Perot antenna and the fully metallic array vs. frequency.

To be more efficient, all achieved results and performances of developed all-metal patch array and Fabry-Perot antenna are numerically summarized in table 1 given below. It present a trade-off between the most important geometrical, mechanical and electrical properties of both designs and what we hope for NASA's interplanetary CubeSat mission. This comparison will help guide future developments in antenna technologies tailored for NASA's interplanetary CubeSat missions, ensuring optimal performance in the harsh environments of space.

Table 1 - Brief summary and geometrical analysis according to NASA's interplanetary CubeSat.

NASA's interplanetary CubeSats	All-Metal Patch Array	Fabry-Perot antenna
2U CubeSat volume	~1.89%	<15%
3U CubeSat volume	~1.26%	~10.4%
6U CubeSat volume	~6.3‰	~5.2%
12U CubeSat Volume	~3.15‰	~2.6%
Lowest Axial Ratio	0.29 dB at 12.1 GHz	~0.6 dB at 12.1 GHz
1dB Axial ratio bandwidth	Ultra-Wide(>300 MHz)	Ultra-Wide(>300 MHz)
Measured gains	35.84 dBi at 11.5 GHz	>20.5 dBi along wide BW

3dB gain bandwidth	Ultra-Wide(>300 MHz)	Ultra-Wide(>300 MHz)
Radiation Pattern	Directional	Directional
Configuration Stiffness	Very High	Very High
EM Interferences/electronics	Negligible	Negligible
Deployment system	No need	No need
Polarization Losses	Negligible	Negligible
Excitation losses	Negligible	Negligible
Overall cost	~ 120 USD	~170 USD

By analyzing these metrics, we can better understand the necessary adjustments and innovations required to enhance communication capabilities for upcoming interplanetary explorations. This understanding will be crucial for designing antennas that meet the specific requirements of NASA's interplanetary CubeSat missions. Ultimately, these advancements will pave the way for more reliable and efficient communication systems, enabling deeper exploration of our solar system and beyond.

4. Fabrication and experimental measurements

The completed all-metal patch array was constructed and evaluated using Agilent Technologies N5247A, US51370362, and A.09.90.02 network analyzers, as well as within an anechoic chamber, as a final and critical step before being installed on the CubeSat. Each of |S11|, |S12|, |S21|, realized gain, and axial ratio properties are tested within a frequency range of 10 to 13 GHz, which is the ideal choice for building high-performance and appropriate-sized CubeSat antennas. Fig. 11 displays the prototype of the created all-metal patch array, as well as its installation within the anechoic chamber with the VNA circuit. Figs. 12 and 13 display the measured |S11|, |S12|, and |S21| parameters of the all-metal patch array prototype as a function of frequency.

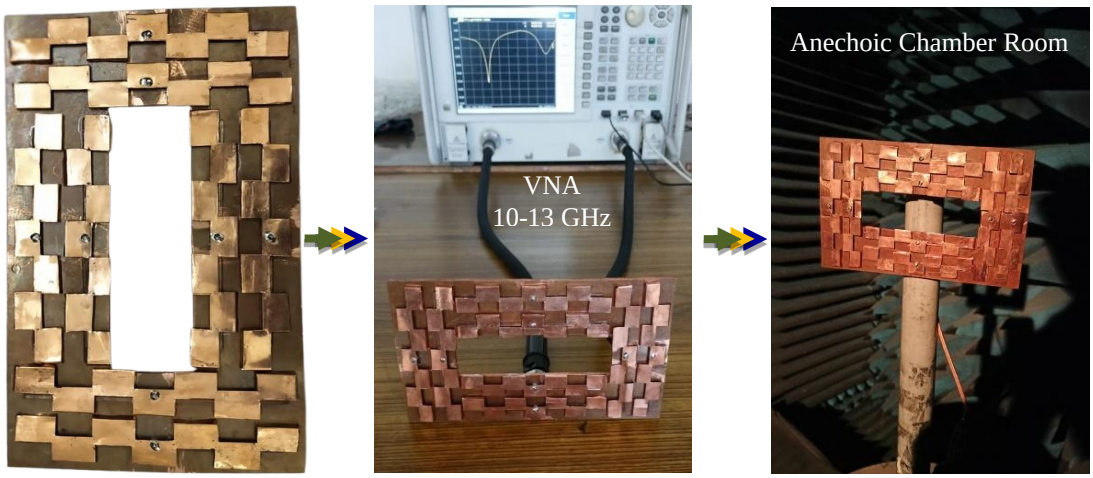

a) Prototype of developed CP all-metal patch array (copper).

b) VNA testing of developed CP all-metal patch array.

c) Anechoic chamber testing of developed CP all-metal patch array.

Fig. 11. Prototype, experiments and measurement setups of prototyped CP all-metal patch array.

Experimental results indicate an impedance bandwidth over 900 MHz, with a reflection coefficient of around -23 dB at 12.1 GHz and the lowest value near -27 dB at 11.92 GHz. Furthermore, for the whole 10-13 GHz (100%) frequency range, the measured |S12| and |S21| are both significantly below -30 dB. The lowest values of |S12| and |S21| are -61.29 dB and -60.68 dB at the same frequency of 11.76 GHz, respectively. The S12 and S21 parameters describe the magneto electric antenna's transmitting and receiving characteristics. Their conclusions are extremely useful since they show a restricted mutual coupling with external components, implying that when parts are closer together, there is less disruption between them. The two curves clearly overlap, confirming the all-metal patch array's strong reciprocity when subjected to a small-signal external magnetic field.

Moreover, Figs. 14 and 15 show the measured findings of realized gain, axial ratio, and 2D radiation patterns derived from anechoic chamber testing. The measured gain is higher than 15 dBi throughout a broad frequency range of around 37% (~10.8-11.9 GHz) and 27% (~12-12.8 GHz), with a peak of 35.84 dBi at 11.5 GHz and a large 3dBi gain bandwidth. This reveals that this lightweight all-metal patch array, and later the PRS-based Fabry-Perot antenna system, provide excellent capabilities for NASA's interplanetary CubeSat missions and supports the simulated findings. These findings highlight how cutting-edge antenna technology might improve deep space exploration's capabilities for telecommunications. The use of such high-performance antennas will be essential for sustaining reliable data transmission and operational efficiency as NASA encourages beyond the constraints of interplanetary missions.

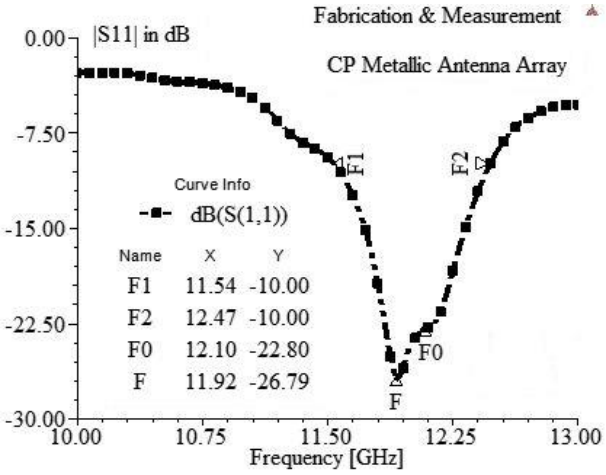

Fig. 12. Measured |S11| coefficient of prototyped CP all-Metal patch array vs. Frequency.

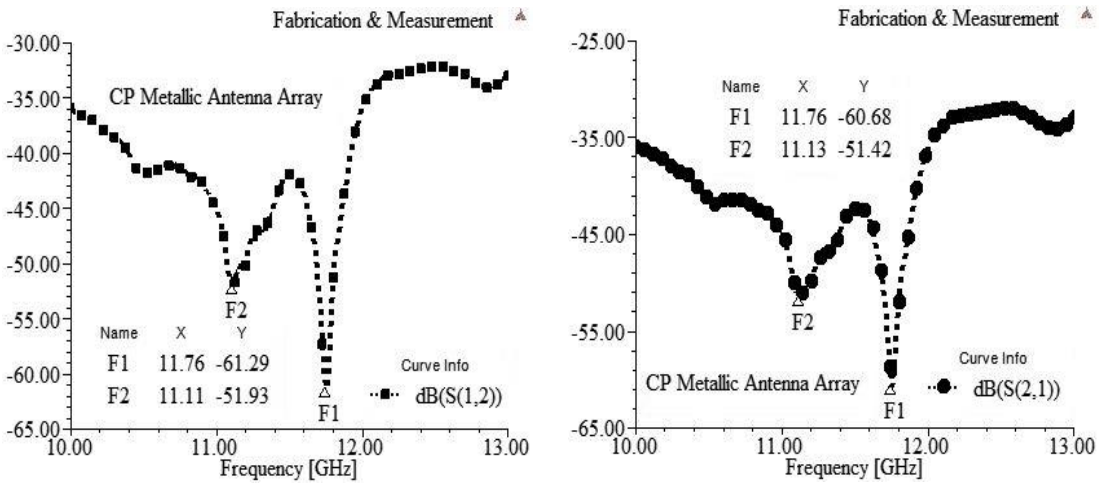

a) Measured |S12| coefficient b) Measured |S21| coefficient

Fig. 13. Measured |S12| and |S21| coefficients of prototyped CP all-Metal patch array vs Frequency.

Moreover, it is found that it is made up of a circularly polarized all-metal patch array, and the measured axial ratio is substantially below 2 dB over the whole frequency range of 10 -13 GHz (100%) and is 0.59, 0.86, and 1.26 dB at 10.77, 12.25, and 12.1 GHz, respectively. This is critical at higher frequencies and for NASA's intended missions since it eliminates all polarization loss probability for an ultra-wide 3dB axial ratio bandwidth (higher than 3GHz). The circular polarization feature of the prototyped all-metal patch array is demonstrated by measurements of the E-field and H-field at 12.25 and 10.77 GHz, as shown in

Fig. 15. The experimental confirmation of the complete techniques provided in this article as a very outstanding and developing option for NASA's interplanetary CubeSat missions is supported by these measurements, which also validate the previously expressed recommendations. It opens the door for next developments in satellite communication architecture in addition to improving communication capabilities in difficult-to-reach places. Solutions like these will be essential to guaranteeing dependable data transfer over long distances as NASA continues to explore new areas of space.

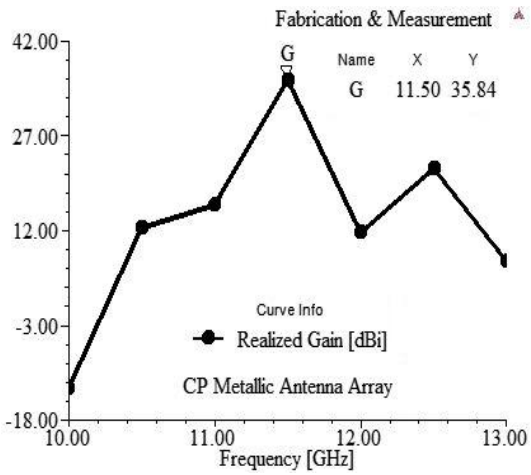

a) Measured realized gain vs frequency.

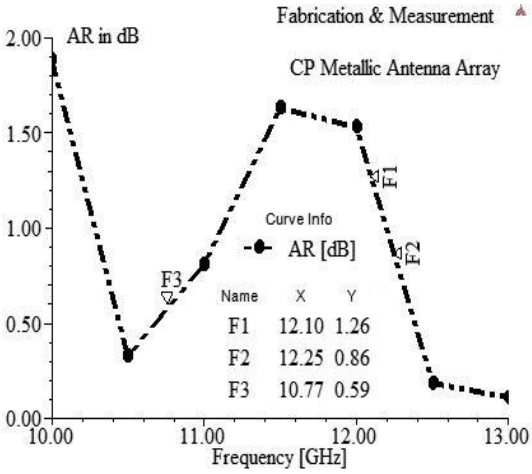

b) Measured axial ratio vs frequency.

Fig. 14. Measured realized gain and axial ratio of prototyped CP all-Metal patch array vs Frequency.

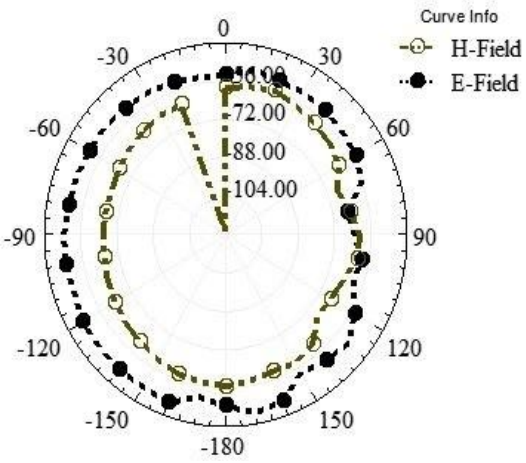

a) Measured 2D Radiation pattern at 12.25 GHz.

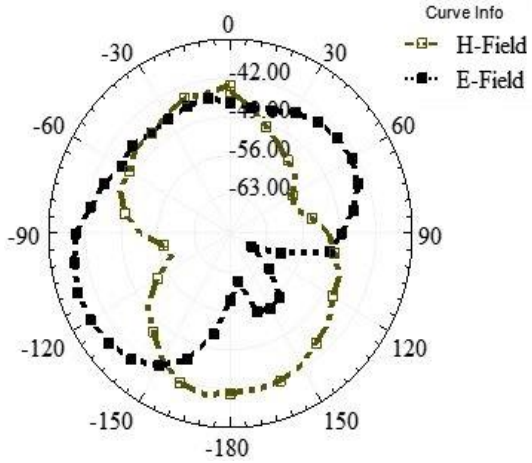

b) Measured 2D Radiation pattern at 10.77 GHz.

Fig. 15. Measured 2D Radiation pattern of prototyped CP all-Metal array at 12.25 and 10.77 GHz.

5. Comparisons with Ku-Band Fabry-Perot antennas and Suitability analysis for NASA's Interplanetary CubeSat Missions

As stated before, the Ku-band frequencies enable the development of small-sized planar antenna designs with excellent performance, stiffness, and, ultimately, efficacy for various AeroCube configurations. In this section, the developed all-metal patch array and the PRS-based Fabry-Perot antennas are compared with more than twenty-two Fabry-Perot antenna designs which are summarized and thoroughly analyzed in terms of physical sizes, materials, unit cell structure, and achieved radiating capabilities, as well as the appropriate CubeSat configuration and interferences with electronic devices inside the CubeSat box. Table 2 illustrates that practically almost all stated FP antenna systems are geometrically and physically acceptable for 2U and 3U configurations and hence all other forms of NASA's interplanetary CubeSats,

requiring no deployment mechanisms. Furthermore, all of the suggested Fabry-Perot arrays are built using PRS unit cells, AMC, MTS, HIS, or parasitic components, which serve as PRS due to their radiating properties. Additionally, all of these FPA designs radiate unidirectionally, resulting in low interference with other electrical components, which eliminates the likelihood of mission failure. They also operate at frequencies spanning from 12.0 to 16.0 GHz, which are appropriate for Fabry-Perot antenna configurations and medium sized CubeSat configurations that provide much space for electronic components. They are printed using low-cost, low-mass dielectric materials such as FR4, Rogers RT Duroid 5880, and Rogers 4003C, which have dielectric constants less than 10 and very low loss tangents (ex., 0.0009 for Rogers Duroid 5880). This makes them cheaper, lighter, consumes less power, and is extremely durable for integration with the CubeSat box or solar cells. However, their overall effectiveness for CubeSat missions with an infinite lifespan, such NASA's interplanetary CubeSat missions depends on their performances around the targeted operating frequencies. More importantly, table 3 shows that these Ku-band Fabry-Perot antenna designs exhibit high gain, with the lowest peak gains of 6.01 and 8.0 dBi discovered in antenna approaches established by (Naik and Vijaya Sri, 2018) and (Sumathi et al., 2021), respectively. Both systems are multiband and linearly polarized, with bandwidths of 1.76 GHz for the first and 854 MHz for the second. As a consequence, these designs may be used for Direct-to-Earth and CubeSat constellation applications with any CubeSat structure if the entire mission is in low Earth orbit. Whilst, they are not suitable for advanced LEO missions of NASA's interplanetary CubeSats owing to the extremely harsh environment in deep space, as well as the extensive distances and speeds of spacecrafts and tiny objects like as comets and asteroids. Despite its dual-band property, circular polarization, and wide 3dB axial ratio bandwidth of 2.2 GHz, the approach presented by (Azizi et al., 2019) can be included with the same recommendations. It gives peak gain below 10 dBi, and its wide 3dB ARBW makes it better than the previews two designs. As a result, this design is recommended for LEO missions, but it cannot be used for NASA's interplanetary CubeSats due to the previously mentioned circumstances.

Table 2 - Geometrical comparison of various Ku-band Fabry-Perot antenna designs.

References	Total Antenna Size	F_0 [GHz]	Materials	FP Unit Cell
Azizi et al., 2019	$1.7\times1.7\times0.41\lambda_{min}^3$	14.125 15.375	RT/D 6002 (ε_r=2.95, 0.762 and 1.542mm-thick), Copper	PRS and HIS
Wu et al., 2020	$3.2\times3.2\times0.53\lambda_0^3$	16	RO4003C (εr=3.38, tanδ= 0.003, 1.524 mm-thick)	PRS
Konstantinidis et al., 2014	$3.86\times3.86\times1.66\lambda_0^3$	14.5	Dielectric (εr= 2.55, 1.6 mm-thick)	PRS
Melouki et al., 2022	$1.72\times1.96\times0.62.\lambda_0^3$	16	Rogers RT/duroid 200 5880 (ε_r=2.2, tanδ=0.0009, 1.575 and 0.787mm-thick)	FSS and PRS
Cao et al., 2019	$1.75\times1.75\times0.775\lambda_0^3$	15	Rogers RT/duroid 200 5880 (ε_r=2.2, tanδ=0.0009, 3 mm-thick), copper	PRS
Abdulkarim et al., 2020	$\sim3.2\times3.2\times0.58\lambda_{min}^3$	12–14.13	FR4 (εr=4.3, tanδ=0.025, 1.6 mm-thick), copper	MTS
Melouki et al., 2022	$\sim2.24\times2.24\times0.768\lambda_0^3$	16	RT/duroid 5880 (ε_r=2.2, tanδ= 0.0009, 1.575 and 0.787mm-thick), Copper	FSS and PRS
Luo et al., 2021	$2.4\times2.4\times0.39\lambda_0^3$ $2.7\times2.7\times0.44\lambda_0^3$	12.45 14.10	dielectric (εr=3.5, 1.5 mm-thick), Aluminum	PRS
Calleau et al., 2019	$5.0\times5.0\times1.0\lambda_0^3$	14.0	HF51 foam	PRS
Omari et al., 2023	$6.878\times6.878\lambda_0^2$	13.4	metallic sheets (0.017mm-thick)	FSS
Mateos-Ruiz et al., 2020	$\sim5.896\times5.896\lambda_0^2$	~15.25	metallic sheets (0.3mm-thick), Eccostock SH foam (ε_r=1, 2mm-thick)	PRS

Liu et al., 2017	$3.2\times3.2\times0.6\lambda_0^3$	13.6	Dielectric (ε_r=2.2, 1.575mm-thick), Copper	MTS
Nguyen & Park, 2015	$5.68\times5.68\times0.47\lambda_0^3$	14.2	Duroid RO4003 (ε_r=3.38, 0.508mm-thick)	FSS
Cao et al., 2018	$1.75\times1.75\times0.75\lambda_0^3$	14	Rogers 5880 (3mm-thick)	PRS
Xiang et al., 2018	$1.45\times1.45\times0.54\lambda_0^3$	14.50	Dielectric (εr>9.8); PEC	AMC
Xie et al., 2019	$2.08\times2.08\times0.95\lambda_{min}^3$	13; 15; 16	Dielectrics (εr_1=10, εr_2=8, εr_3=6, εr_4=4)	PRS
Sumathi et al., 2021	$0.95\times0.95\times0.85\lambda_0^3$	15.54	Roger RT Duroid 5880 (εr= 2.2, tanδ= 0.0009, 1.5-mm-thick), Copper	MTM
Ge & Qin, 2018	$\sim1.6\times1.6\times0.66\lambda_{min}^3$	12 - 12.8	F4B (ε_r=2.55), F4B (ε_{r1}=4.5, ε_{r2}=13, 2.5 and 4mm-thick)	PRS
Meriche et al., 2019	$\sim2.95\times2.95\times0.7\lambda_0^3$	15.0	Rogers 4003C (ε_r=3.38, tanδ=0.003, 1.53mm-thick); Copper	PRS
Yang et al., 2018	$\sim4.26\times4.26\times0.46\lambda_{min}^3$	12.8; 13.2	Rogers RT5880 (ε_r=2.2, 0.787 and 2mm-thick)	FSS and PRS
Niaz et al., 2020	$\sim2.4\times2.4\times0.66\lambda_0^3$	13.40	Rogers RT5880 (ε_r=2.2 and tanδ=0.0009, 0.787mm-thick)	PRS
Naik & Vijaya Sri, 2018	$1.82\times2.187\times0.9\ \lambda_{min}^3$	13.67; 15.28	FR4 (ε_r=4.4, tanδ=0.025, 1.59mm-thick); Copper	Parasitic elements
All-Metal Patch Array	$4.5\times6.13\times0.08\lambda_0^3$	10-13; 12.1	Only Copper	Cross-Array
Fabry-Perot Antenna	$4.5\times6.13\times\lambda_0^3$	10-13; 12.1	Copper; Rogers RT5880 (ε_r=2.2, 2mm-thick)	cross-Array; PRS

The antenna techniques given by (Cao et al., 2019), (Callean et al., 2019), and (Ge and Qin, 2018) demonstrate that these antenna systems work on a single effective band, are circularly polarized, and have minimal power consumption. Furthermore, the first one has a very wide 3dBi gain bandwidth extending from 12.4 to 16.8 GHz and a 3dB ARBW of 11.7-17.2 GHz. However, their actual gains are insufficient to make them suitable candidates for advanced LEO CubeSat or NASA's interplanetary CubeSat missions. The antenna designs provided by (Wu et al., 2020), (Melouki et al., 2022), (Liu et al., 2017), (Nguyen & Park, 2015), (Cao et al., 2018), (Xie et al., 2019), (Meriche et al., 2019), and (Niaz et al., 2020) show exceptionally broad 3 dBi gain bandwidths at Ku-band with average peak gains close to 16.0 dBi. Furthermore, the techniques of Wu et al. (2020), Liu et al. (2017), and Nguyen & Park (2015) demonstrate realized gains of 18.38, 17.90, and 18.5 dBi, respectively. They are excellent prospects for advanced LEO CubeSat flights, but linear polarization and middling gains restrict their suitability for NASA's interplanetary CubeSat programs. They will exhibit large polarization losses, and the corresponding CubeSat configuration may make them unsuitable for NASA's interplanetary missions using tiny spacecraft. The antenna systems described by (Abdulkarim et al., 2020), (Luo et al., 2021), and (Xiang et al., 2018) are linearly polarized, operate over a wide range of effective bands, and provide an average gain of almost 14.0 dBi at Ku-band. Furthermore, their lightweight design, excellent rigidity, and low power consumption make them ideal candidates for small advanced LEO CubeSats. While the extremely hard conditions of the deep space environment demonstrate that their capabilities are insufficient to target NASA's interplanetary CubeSat missions. In terms of realized gain, which is one of the most important antenna characteristics for interplanetary CubeSat applications, the approaches introduced by (Konstantinidis et al., 2014), (Mateos-Ruiz et al., 2020), and (Yang et al., 2018) provide peak gains very close to 20.0 dBi at Ku-band and operate over wide impedance bandwidths. As a result, if polarization difficulties are ignored, these antenna designs can be employed in advanced LEO missions and mother-daughter interplanetary missions when the mother spacecraft possesses a strong circularly polarized antenna system.

Table 3 - Performances of various Ku-band Fabry-Perot antennas and suitability analysis for NASA's interplanetary CubeSats.

References	F_0[GHz]	Peak Gain	Bandwidths [GHz]	Polarization	NASA's CubeSat	EM Interference
Azizi et al., 2019	14.125 15.375	10 9.2	3dB ARBW: 13.5-15.7 -10dB BW: 13.8-14.2 &15.3-15.6	Circular	2U 3U	Minimum
Wu et al., 2020	16	18.38	-10dB BW: 14.8 -18.5 3dBi gain BW: 14.6–16	Linear	2U 3U	Minimum
Konstantinidis et al., 2014	14.5	20.0	-10dB BW: ~13.7-15.2	Linear	2U 3U	Minimum
Melouki et al., 2022	16	14.72	-10dB BW: 11.32-17.35 3dB gain BW: 11.68-16.78	Linear	2U 3U	Minimum
Cao et al., 2019	15	11.45	-10dB BW: 11.7-19.8 3dB ARBW: 11.7-17.2 3dB gain BW: 12.4-16.8	Circular	2U 3U 6U	Minimum
Abdulkarim et al., 2020	12–14.13	14.20	-10dB BW: 2.13 (12–14.13)	Linear	2U 3U	Minimum
Melouki et al., 2022	16	14.21	-10dB BW: 11.9-17.6 3dB gain BW: 11.6-17.24	Linear	2U 3U	Minimum
Luo et al., 2021	12.45 14.10	14.30 16.80	-10dB BW: ~1.2-12.6 ~13.6-14.5	Vertical Horizontal	2U 3U	Minimum
Calleau et al., 2019	14.0	~13.0	-10dB BW: 12.8-16 3dB ARBW: 12-16	Circular	2U 3U	Minimum
Omari et al., 2023	13.4	15.5	-10dB BW: 13.33-13.44; 13.53-13.93 and 13.94 – 15.0	Linear	6U 8U 12U	Minimum
Mateos-Ruiz et al., 2020	~15.25	20.6	-10dB BW: 0.97	Linear	2U 3U	Minimum
Liu et al., 2017	13.6	17.90	-10dB BW: ~13.6-13.7 3dB gain BW: 12.2-14.9	Linear	2U 3U	Minimum
Nguyen & Park, 2015	14.2	18.5	-10dB BW: 13.9–15.8 3dB gain BW: 13.8–14.8	Linear	6U 8U 12U	Minimum
Cao et al., 2018	14	11.2	-10dB BW: 11.5-18.7 3dB gain BW: 12.3- 17.2	Linear	2U 3U	Minimum
Xiang et al., 2018	14.50	13.70	-10 dB BW: ~14.20 - 14.70	Linear	2U 3U	Minimum
Xie et al., 2019	13; 15; 16	17.30	3-dB gain BW: ~10-14.5	Linear	2U 3U	Minimum
Sumathi et al., 2021	15.54	~8.0	-10 dB BW: 1.76	Linear	2U 3U	Minimum
Ge & Qin, 2018	12 - 12.8	16.30	10 dB BW: 12-13.8 3dB ARBW: 11.8-13.3	Circular	2U 3U	Minimum
Meriche et al., 2019	15.0	13.78	3dB gain BW: 12.6-15.2 -10 dB BW: 13.1-15.3	Linear	2U 3U	Minimum
Yang et al., 2018	12.80; 13.20	19.10	-10 dB BW:~12.7-13.5	Linear	2U 3U	Minimum
Niaz et al., 2020	13.40	14.00	-10 dB BW:~10.5-15.5 3dB gain BW: 11.2-15.4	Linear	2U 3U	Minimum
Naik & Vijaya Sri, 2018	13.67; 15.28	8.01 6.01	-10 dB BW: 0.854 (13.179–14.033) and 1.14 (14.584–15.724)	Linear	2U 3U 6U	Minimum
All-Metal Patch Array	10-13; 12.1	35.84	3dB ARBW: 10-13 -10 dB BW:10.4-11.3 & 11.6-12.8	Circular	2U 3U 6U	Minimum
Fabry-Perot Antenna	10-13; 12.1	>22	-10 dB BW:10.4-12.7	RHCP and LHCP	2U 3U	Minimum

	AR of 0.29 dB	6U

Omari et al. (2023) designed a triband Fabry-Perot antenna system with exceptionally low power consumption. It does not require any deployment equipment, can be created rapidly, achieves a peak gain of 15.5 dBi at Ku-band, and is entirely comprised of metal, making it an extremely rigid and lightweight antenna system. As a result, it is suitable for advanced LEO missions and interplanetary CubeSats with a strong circularly polarized antenna system on the mothership or earth station. Henceforth, almost all Fabry-Perot antenna systems are no longer appropriate for NASA's interplanetary CubeSat missions, as they place significant demands on the mother spacecraft and earth station antennas. This means that the all-metal patch array alone, as well as the Fabry-Perot antenna systems developed in this article, have the highest realized gains, the lowest axial ratio, wide 3dB axial ratio bandwidths, high stiffness, and low power consumption, making them ideal candidates for NASA's interplanetary CubeSat without any deployment system or hard conditions on the mothership and earth station antenna systems, despite the harsh environment beyond Earth.

For instance, it is better to take into account the lengthy inquiry presently underway by NASA to determine the circumstances that led to the termination of Ingenuity's missions, which were created by our friends at NASA, and to examine the lessons learnt from its historic experience. Ingenuity was initially sent to Mars as part of the Perseverance mission as an experimental tool to test the feasibility of flying on another planet, but it has exceeded expectations and has evolved into an important exploration tool that assists the Perseverance rover in exploring the desert environment of Jezero Crater (Balaram et al., 2021) (Veismann et al., 2021). During its three-year mission, Ingenuity conducted 72 flights on Mars, gathering critical scientific data. During its final flight, the helicopter soared 12 meters (40 feet) above the surface of Mars before descending back to the ground after 32 seconds of flight. Following that, NASA scientist Howard Gripp explains that when looking into an accident from 100 million miles away, there are no eyewitnesses or black boxes, and the most likely cause is the navigation system's lack of information because of Mars' soft surface. This illustrates how effective, inexpensive, and stiff antenna systems such as the very high gain circularly polarized all-metal patch array and the PRS-based Fabry-Perot Antenna systems developed through this project can be in helping NASA enhance the performance of its small/medium sized spacecrafts, like Ingenuity. Furthermore, the achieved results show that only-metal and Fabry-Perot antenna systems are the best option for replacing large reflector or deployable antenna systems used by NASA and other space agencies like ESA and JAXA to target interplanetary CubeSat missions. These antenna configurations, with their features and capabilities, bridge the gap between university research and national/private space agencies, minimizing total mission costs and development time. This raises the mission's success rate while keeping costs low, making the discovery field and beyond-earth environment particularly interesting to university students.

Because of these NASA achievements, as well as its partnerships with SpaceX and Blue Origin, small spacecraft like interplanetary CubeSats are crucial to the completion of the whole space program, including NASA's ARTEMIS II (Creech et al., 2022). This project aims to explore the potential for human exploration of Mars and beyond by utilizing state-of-the-art technology and partnerships to enhance its capabilities. By using the benefits of CubeSat spacecraft with a mothership to accomplish the maximum achievement conceivable, NASA is paving the way for more cost-effective and efficient space exploration. Why not move on to make human life multiplanetary? It is a clear and open invitation to all scholars at institutions worldwide to join in this global purpose of mankind. We are from our region, and by concentrating on the creation of inexpensive, low-power, and intelligent Fabry-Perot antenna configurations, we validate this NASA request and inform the scientific community that it is not as difficult as it seems. It is a part of our responsibility to future generations. We must ensure that we leave behind a sustainable world, rich in resources and opportunities, allowing them to thrive and enjoy a quality of life that we have come to cherish.

6. Conclusions

NASA's interplanetary CubeSats have given rise to a cutting-edge research business that is changing the field. It is possible that this new mission development philosophy will alter the interplanetary exploration economics. To go to its destination in the Solar System, each CubeSat was transported as a mother-daughter pair. Each offered a special skill that may have improved the mission's overall science. Some offered in situ measurements, while others conducted flybys of the target body to get a closer view than might be possible with the primary spacecraft. This paper evaluates suitable antenna systems for NASA's interplanetary CubeSats. The designed antenna system is an all-metal patch array with a single PRS layer adapted to create a high gain circularly polarized Fabry-Perot antenna system suitable for NASA's interplanetary CubeSats.This all-metal patch array was well-fabricated and tested using a VNA and an anechoic chamber, resulting in good agreement with simulated findings.The measured findings reveal that it is circularly polarized, providing a realized gain of 35.84 dBi and an AR of 1.629 dBi at 11.5 GHz, with a 3-dB AR bandwidth greater than 3.0 GHz around 11.5 GHz. It also indicates that the measured |S12| and |S21| coefficients are significantly below -30 dB throughout a large frequency band ranging from 10.0 to 13.0 GHz, with a low |S11| parameter of -22.80 dB at 12.1GHz.It was also found that the single layer PRS-based Fabry-Perot configuration enhances the achieved realized gain while also increasing the axial ratio and the impedance bandwidth. Along with having RHCP and LHCP capabilities, it works on a broad effective band that spans 10.4 to 12.7 GHz, has an AR of 0.29 dB and input impedance very close to 50Ω (49.9-j0.1) at 12.1 GHz. All of this demonstrates how successful the strategy described in this work for its use in NASA's interplanetary CubeSat missions, which allowed NASA to open and lead the way for space exploration employing small-scale technologies.

References

Abdulkarim, Y. I., Awl, H. N., Muhammadsharif, F. F., Karaaslan, M., Mahmud, R. H., Hasan, S. O., Işik, Ö., Luo, H., & Huang, S. (2020). A low-profile antenna based on single-layer metasurface for Ku-band applications. *International Journal of Antennas and Propagation*, 2020(1), 8813951. https://doi.org/10.1155/2020/8813951

Autry, G. (2024). The United States in space: Strategies, capabilities, and vision. *Asia Policy*, 19(4), 6–18. https://doi.org/10.1353/asp.2024.a942827

Azizi, Y., Komjani, N., Karimipour, M., & Aryanian, I. (2019). Demonstration of a self-polarizing dual-band single-feed circularly polarized Fabry–Perot cavity antenna with a broadband axial ratio. *AEU - International Journal of Electronics and Communications*, 111, 152909. https://doi.org/10.1016/j.aeue.2019.152909

Balaram, J., Aung, M., & Golombek, M. P. (2021). The Ingenuity helicopter on the Perseverance rover. *Space Science Reviews*, 217(1), 56. https://doi.org/10.1007/s11214-021-00815-w

Benhmimou, B., Omari, F., Gupta, N., El Khadiri, K., Ahl Laamara, R., & El Bakkali, M. (2024). Air-gap reduction and antenna positioning of an X-band bow tie slot antenna on 2U CubeSats. *Journal of Applied Engineering and Technological Science*, 6(1), 86–102. https://doi.org/10.37385/jaets.v6i1.6158

Calleau, A., García-Vigueras, M., Legay, H., Sauleau, R., & Ettorre, M. (2019). Circularly polarized Fabry–Perot antenna using a hybrid leaky-wave mode. *IEEE Transactions on Antennas and Propagation*, 67(9), 5867–5876. https://doi.org/10.1109/TAP.2019.2920266

Campana, C. T. (2023). Interplanetary trajectory design in high-fidelity model: Application to deep-space CubeSats' cruises. *Materials Research Proceedings*, 33, 185–192. https://doi.org/10.21741/9781644902677-27

Cao, W., Lv, X., Wang, Q., Zhao, Y., & Yang, X. (2019). Wideband circularly polarized Fabry–Pérot resonator antenna in Ku-band. *IEEE Antennas and Wireless Propagation Letters*, 18(4), 586–590. https://doi.org/10.1109/LAWP.2019.2896940

Cao, W., Wang, Q., Jin, J., & Li, H. (2018). Magneto-electric dipole antenna (MEDA)-fed Fabry–Perot resonator antenna (FPRA) with broad gain bandwidth in Ku band. *IEEE Access*, 6, 65557–65562. https://doi.org/10.1109/ACCESS.2018.2878054

Creech, S., Guidi, J., & Elburn, D. (2022). Artemis: An overview of NASA's activities to return humans to the Moon. In *2022 IEEE Aerospace Conference (AERO)* (pp. 1–7). IEEE.

El Bakkali, M., El Bekkali, M., Gaba, G. S., Guerrero, J. M., Kansal, L., & Masud, M. (2021). Fully integrated high gain S-band triangular slot antenna for CubeSat communications. *Electronics*, 10(2), 156. https://doi.org/10.3390/electronics10020156

Freeman, A. (2020). Exploring our solar system with CubeSats and SmallSats: The dawn of a new era. *CEAS Space Journal*, 12(4), 491–502. https://doi.org/10.1007/s12567-020-00298-5

Ge, Y., & Qin, K. (2018). Wideband high-gain circularly polarised antenna based on Fabry–Perot concept and a conical horn. In *12th European Conference on Antennas and Propagation (EuCAP 2018)* (pp. 1–3). https://doi.org/10.1049/cp.2018.0614

Kramer, D. (2021). The undermining of science is Trump's legacy. *Physics Today*, 74(3), 24–27. https://doi.org/10.1063/PT.3.4697

Lambright, W. H. (2024). Leading the Moon to Mars program: James Bridenstine as NASA administrator 2018–2021. *Space Policy*, 68, 101634. https://doi.org/10.1016/j.spacepol.2024.101634

Liu, Z. G., Lu, W. B., & Yang, W. (2017). Enhanced bandwidth of high directive emission Fabry–Perot resonator antenna with tapered near-zero effective index using metasurface. *Scientific Reports*, 7, 11455. https://doi.org/10.1038/s41598-017-11141-z

Luo, C. W., Jiao, Y. C., Zhao, G., & Chen, G. T. (2021). Novel low-profile dual-band and dual-polarization Fabry–Perot resonator antenna. *International Journal of RF and Microwave Computer-Aided Engineering*, 31(4), e22566. https://doi.org/10.1002/mmce.22566

Mateos-Ruiz, P., Hernández-Escobar, A., Abdo-Sánchez, M. E., & Camacho-Peñalosa, C. (2020). Design and fabrication of a Fabry–Pérot cavity antenna for the Ku-band. In *XXXV Simposium Nacional de la Unión Científica Internacional de Radio* (pp. 1–4). https://hdl.handle.net/10630/19799

Melouki, N., Hocini, A., & Denidni, T. A. (2022). High gain and wideband Fabry–Perot resonator antenna based on a compact single PRS layer. *IEEE Access*, 10, 96526–96537. https://doi.org/10.1109/ACCESS.2022.3205605

Melouki, N., Hocini, A., & Denidni, T. A. (2022). High-gain and wideband Fabry–Perot resonator antenna based on a pixelated single PRS layer for Ku-band applications. In *2022 IEEE International Symposium on Antennas and Propagation and USNC-URSI Radio Science Meeting* (pp. 988–989). https://doi.org/10.1109/AP-S/USNC-URSI47032.2022.9887266

Meriche, M. A., Attia, H., Messai, A., Mitu, S. S. I., & Denidni, T. A. (2019). Directive wideband cavity antenna with single-layer meta-superstrate. *IEEE Antennas and Wireless Propagation Letters*, 18(9), 1771–1774. https://doi.org/10.1109/LAWP.2019.2929579

Naik, K. K., & Vijaya Sri, P. A. (2018). Design of hexadecagon circular patch antenna with DGS at Ku band for satellite communications. *Progress in Electromagnetics Research M*, 63, 163–173. https://doi.org/10.2528/PIERM17092205

Niaz, M. W., Yin, Y., Bhatti, R. A., Cai, Y. M., & Chen, J. (2020). Wideband Fabry–Perot resonator antenna employing multilayer partially reflective surface. *IEEE Transactions on Antennas and Propagation*, 69(4), 2404–2409. https://doi.org/10.1109/TAP.2020.3022555

Nguyen, T. K., & Park, I. (2015). Broadband single-feed microstrip antenna in a Fabry–Perot resonator. In *2015 International Workshop on Antenna Technology (iWAT)* (pp. 333–334). https://doi.org/10.1109/IWAT.2015.7365276

Omari, F., Benhmimou, B., Hussain, N., Laamara, R. A., Arora, S. K., Guerrero, J. M., & Bakkali, M. E. (2023). UM5 of Rabat to deep space: Ultra-wide band and high-gain only-metal Fabry–Perot antenna for interplanetary CubeSats in IoT infrastructure. In *Low Power Architectures for IoT Applications* (pp. 153–164). Springer. https://doi.org/10.1007/978-981-99-0639-0_8

Patidar, H., Das, A., & Kar, R. (2024). Small planar antenna array design using length and spacing through MATLAB–HFSS interfacing. *International Journal of Communication Systems*, 37(9), e5770. https://doi.org/10.1002/dac.5770

Sumathi, K., Lavadiya, S., Yin, P., Parmar, J., & Patel, S. K. (2021). High-gain multiband and frequency-reconfigurable metamaterial superstrate microstrip patch antenna for C/X/Ku-

band wireless network applications. *Wireless Networks*, 27, 2131–2146. https://doi.org/10.1007/s11276-021-02567-5

Tanaka, T., Ebinuma, T., Nakasuka, S., Matsumoto, T., Sobukawa, R., & Aoyanagi, Y. (2024). Systems design results of LunaCube: Dual-satellite lunar navigation system with 6U-CubeSats. *Acta Astronautica*, 216, 318–329. https://doi.org/10.1016/j.actaastro.2023.11.026

Thompson, M. R., Forsman, A., Chikine, S., Peters, B. C., Ely, T., Sorensen, D., Parker, J., & Cheetham, B. (2022). Cislunar navigation technology demonstrations on the CAPSTONE mission. In *Proceedings of the 2022 International Technical Meeting of The Institute of Navigation* (pp. 471–484). https://doi.org/10.33012/2022.18208

Tollefson, J., Maxmen, A., Remmel, A., Subbaraman, N., & Witze, A. (2021). Joe Biden pursues giant boost for US science spending. *Nature*, 592(7855), 498–499. https://doi.org/10.1038/d41586-021-00897-0

Veismann, M., Dougherty, C., Rabinovitch, J., Quon, A., & Gharib, M. (2021). Low-density multi-fan wind tunnel design and testing for the Ingenuity Mars helicopter. *Experiments in Fluids*, 62(9), 193. https://doi.org/10.1007/s00348-021-03278-5

Wu, T., Chen, J., & Wu, P. F. (2020). Broadband and multi-mode Fabry–Pérot cavity antenna with gain enhancement. *AEU - International Journal of Electronics and Communications*, 127, 153440. https://doi.org/10.1016/j.aeue.2020.153440

Xiang, X. Z., Liu, Z. G., & Lu, W. B. (2018). Small-aperture and low sidelobe-level Fabry–Perot resonator antenna. In *2018 IEEE Asia-Pacific Conference on Antennas and Propagation (APCAP)* (pp. 292–293). https://doi.org/10.1109/APCAP.2018.8538128

Xie, J., Qin, F., Cheng, W., Zhang, H., & Gao, S. (2019). A design of extremely wideband Fabry-Perot cavity antenna. In *2019 IEEE International Conference on Computational Electromagnetics (ICCEM)* (pp. 1–3). https://doi.org/10.1109/COMPEM.2019.8779075

Yang, J., Xu, F., & Yao, S. (2018). A dual-frequency Fabry–Perot antenna based on metamaterial lens. In *12th International Symposium on Antennas, Propagation and EM Theory (ISAPE)* (pp. 1–3). https://doi.org/10.1109/ISAPE.2018.8634017